Environmental Pollution
December 2022, Volume 315 Pages 120383 (9p.)
https://doi.org/10.1016/j.envpol.2022.120383
https://archimer.ifremer.fr/doc/00797/90909/

Cryogrinding and sieving techniques as challenges towards producing controlled size range microplastics for relevant ecotoxicological tests

Gardon Tony [1, *], Paul-Pont Ika [2], Le Moullac Gilles [1], Soyez Claude [1], Lagarde Fabienne [3], Huvet Arnaud [4]

[1] Ifremer, ILM, IRD, Univ Polynésie Française, UMR EIO, F-98719, Taravao, Tahiti, Polynésie Française, France
[2] Univ Brest, Ifremer, CNRS, IRD, LEMAR, F-29280, Plouzané, France
[3] Institut des Molécules et Matériaux du Mans, IMMM - UMR CNRS 6283, Le Mans Université, Avenue Olivier Messiaen, 72085, Le Mans, France
[4] Univ Brest, Ifremer, CNRS, IRD, LEMAR, F-29280, Plouzané, France

* Corresponding author : Tony Gardon, email address : tony.gardon@ifremer.fr

Abstract :

The impact of microplastics (MP) has attracted much attention from the scientific community and many laboratory assessments have been made of their effects on aquatic organisms. To produce MP from real environmental plastic waste, which would enable more realistic experiments, we used plastic pearl farming equipment from French Polynesian lagoons. Here, the pearl oyster Pinctada margaritifera could encounter MP coming from their breakdown in its surrounding environment. We tested an established method based on mechanical cryogenic grinding and liquid sieving. Our desired size range was 20–60 μm, corresponding to the optimal particle size ingested by P. margaritifera. The protocol was effective, generating MP particles of 20–60 μm (~17,000–28,000 MP μg−1), but also produced too many smaller particles. The peak in the desired size range was thus flattened by the many small particles <3 μm (~82,000–333,000 MP μg−1; 53–70% of total analysed particles), visible at the limit of Coulter counter analysis (cut-off point: 2 μm). Laser diffraction analysis (cut-off point: 0.4 μm) provided greater detail, showing that ~80–90% of the total analysed particles were <1 μm. Diverging particle size distributions between those expected based on sieving range and those really observed, highlight the need to perform fine-scaled particle size distribution analyses to avoid underestimating the number of small micro- and nanoplastics (MNP) and to obtain an exact estimation of the fractions produced. Size and microstructure characterization by scanning electron microscopy suggested spontaneous particle self-assembly into crystal superstructures, which is the supposed cause of the divergence we observed. Overall, our results emphasize that particle self-assembly is a technical hurdle requiring further work and highlight the specific need to finely characterize the size distribution of MNP used in ecotoxicological experiments to avoid overestimating effects.

Graphical abstract

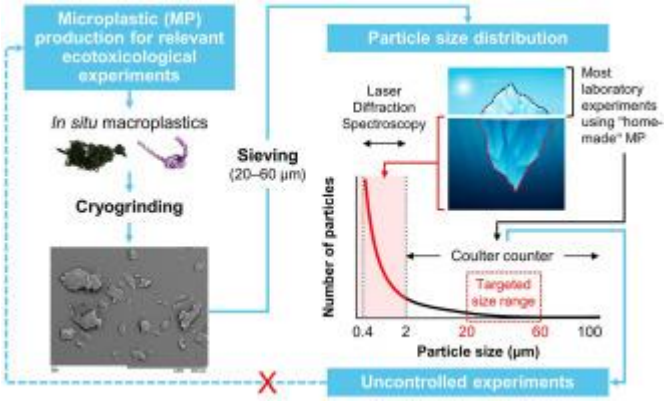

Highlights

► “Homemade” microplastics may underestimate exposure level and overestimate impact. ► Particle sieving range was inconsistent with size distribution. ► Particle self-assembly may cause biased sieving and size distribution. ► Particle size distribution needs to be systematically characterized very finely. ► For standardization, it is vital to improve microplastic manufacture and sizing.

Keywords : Laboratory experiment, Microplastic production, Sieving, Particle self-assembly, Uncontrolled size distribution, Underestimated concentration

1. Introduction

Microplastic particles (MP, <5 mm) are the most numerically abundant form of solid waste on Earth (Eriksen et al., 2014). Over the past fifteen years, the scientific community has studied this global concern by evaluating environmental concentrations in different marine compartments (Eriksen et al., 2014; Cózar et al., 2014; Woodall et al., 2014; van Sebille et al., 2015), as well as the adverse effects on aquatic organisms in laboratory conditions (reviewed in Thornton Hampton et al., 2022). Historically, the vast majority of laboratory experiments used a single polymer type, in pieces of spherical shape (*i.e.* microbeads), and particle concentrations mostly higher (in number of particles per volume) than those found in the field (Phuong et al., 2016; Lenz et al., 2016). These biases were mainly caused by a lack of more appropriate polymer types and shapes, and uncertainties regarding *in situ* concentrations of particles below 300 µm. Although an increasing number of papers now aim to consider the heterogeneity of microplastics (*i.e.* by including a variety of particle shapes, sizes, polymer types, surface properties; Rochman et al., 2019), the gap between potential and actual risks remain concrete considering the lack of relevance in ecological terms (Connors et al., 2017; de Sá et al., 2018).

A rigorous understanding of the environmental impacts of MP on marine biota requires fine evaluation of concentrations and characteristics of the smallest MP sizes in order to conduct relevant environmental experiments in laboratory conditions. The first step to using more realistic MP scenarios is to conduct an evidence-based approach, which means targeting the most relevant particles in terms of shape (*i.e.* fragments rather than spheres), size (*i.e.* polydisperse rather than monodisperse), polymers (*i.e*. those mostly found locally), and surface properties (*i.e.* aging and biofilm). For instance, recent studies demonstrating physical and chemical differences between weathered plastics and pristine ones or post-production consumer products have highlighted the need to use materials for ecotoxicology tests that are as similar

as possible to those found *in situ* (Jahnke et al., 2017). Using collected weathered plastics, such as beached macroplastic litter, to produce MP therefore offers a way to obtain relevant test materials for impact assessment studies (Kühn et al., 2018).

In the lagoons of French Polynesia, pearl farming has been identified as a specific source of plastic pollution through the accumulation of operational and abandoned plastic equipment (*e.g.* ropes, collectors, buoys) (Andréfouët et al., 2014). A recent monitoring study in pearl farming lagoons revealed a widespread contamination by MP in both seawater and cultured pearl oyster (Gardon et al., 2021). Among the possible ecological disturbances discussed in Andréfouët et al. (2014), one comes from a preliminary experiment conducted by Gardon et al. (2018) highlighting a dose effect of polystyrene microbeads on energy balance (Gardon et al., 2018) and dose-specific transcriptomic disruption of gene expression (Gardon et al., 2020b) in the pearl oyster (*Pinctada margaritifera*). As *P. margaritifera* is a species of commercial interest and the second most important economic resource in French Polynesia, risk assessment using realistic MP (*i.e.* sourced from local pearl-farming gear debris) is very important. It will form the crucial next step to improving both the simulation of the pearl oyster environment and the realism of results that can support decision making.

A few recent studies provide protocols for preparing model micro- and nanoplastics (*e.g.* Cole, 2016; Eitzen et al., 2019), some of which present cryomilling as an effective way to obtain reference particles (Kühn et al., 2018). However, the particles thus-obtained from aged polymers were mostly in the range of several hundred µm (Kühn et al., 2018) or nano sized (El Hadri et al., 2020). The production of standardized size particles targeting a range of around 1 to 100 µm, which is a typical size range used in most of laboratory studies (de Sá et al., 2018; Paul-Pont et al., 2018), remains under-investigated. The present analytical investigation thus proposes to test a cryogrinding and sieving protocol for laboratory MP production from weathered plastic pearl farming equipment as this is a potential source of MP in pearl farming

lagoons (Gardon et al., 2021). The objective was to obtain a specific size range of particles included in the *P. margaritifera* particle size retention range (2 to 200 µm; Pouvreau et al., 1999). Thus, in view of our environmental data showing the prevalence of MP 20–200 µm in the cultured pearl oysters (Gardon et al., 2021) and to keep close to the most MP size used in laboratory studies (<50 µm; de Sá et al., 2018), we focused on the obtention of polydisperse particles ranging from 20 to 60 µm. With the aim of questioning difference between the expected and the real particle sizes, we hypothesized that cryogrinding and sieving techniques do not make it possible to obtain a specific particle size range regardless of the grinding time. Yet, this approach has already been used in some recent (eco)toxicological studies (*e.g.* Revel et al., 2019; Schür et al., 2020; Carrasco-Navarro et al., 2021). However, the overall particle size distribution of the obtained plastic powder was not always considered, depending on the method used to characterize these "lab MP". A commonly used approach is a Coulter counter equipped with a 100 µm aperture tube, which allows the detection of particles ranging from 2 to 100 µm (Revel et al., 2019; Schür et al., 2020; Zimmermann et al., 2020), while the number of particles <2 µm remains unknown if no further analysis is performed. The lack of consideration of the smaller size range is therefore an omission that deserves attention. In our study, we examine the potential scale of the error caused by ignoring the nano fraction. This would bias ecotoxicological results interpretation, especially considering that the toxicity of particles increases as their size decreases (Jeong et al., 2016; Ma et al., 2016). We demonstrate the need to improve the standardization of particle concentrations used in exposure experiments and highlight the real challenges of producing microplastics with a controlled size range.

2. Materials and methods

2.1. Plastic selection

Several types of plastic pearl farming gear were collected from a pearl farm in Manihi atoll (14°24′10.4″S, 145°57′29.2″W), among which synthetic ropes and spat collectors were the most abundant (Andréfouët et al., 2014). Both ropes and collectors are suspected to be potential sources of polyethylene (PE) and polypropylene (PP) microplastics in the environment of cultivated pearl oysters (Gardon et al., 2021). The polymers of the gear were identified by Fourier-transform infrared spectroscopy (FTIR) on both plastic pieces and MP particles produced, confirming that the spat collector (shade-mesh) was made of PP (**Figure 1**A–B) and the rope was made of PE (**Figure 1**D–E).

2.2. Microplastic production

The sampled spat collectors and ropes were first washed in saline water (100 g of NaCl L^{-1}) overnight (o/n) to remove as many potentially present microorganisms as possible, then rinsed thoroughly and dried at 60°C for 3 days in a proofer. They were then cut into ≤1 cm pieces using clean stainless-steel scissors (**Figure 1**C and F; **Figure 2**, step 1). A second washing in saline water was performed o/n on the plastic pieces, followed by rinsing with filtered (1.2 µm) distilled water and drying in a proofer at 60°C for 3 days. Two-gram aliquots of dried plastic pieces were packaged in aluminium and immersed in liquid nitrogen for mechanical cryogenic grinding. Steel grinding jars (50 ml) with a steel ball 2 cm in diameter were cooled in liquid nitrogen and filled with an aliquot (2 g of plastic pieces per jar) once all materials were cooled down (**Figure 2**, step 2). The grinding jars were then placed in a Mixer Mill MM 400 (Retsch™) for grinding (**Figure 2**, step 3). Three running times were tested for each MP type: 1-, 2- and

153 3-minutes run of grinding. After grinding, the MP from the spat collector (MP_{coll}) and rope
154 (MP_{rope}) were dried at 60°C o/n before sieving (**Figure 2**, step 4).
155 A multi-step sieving phase was carried out to collect the MP 20–60 µm fraction. First, the MP
156 powder was sieved through the 60 µm sieve and rinsed with filtered 70% ethanol from a wash
157 bottle, aiming to avoid MP aggregates as much as possible and facilitate particle passage
158 through the sieve (**Figure 2**, step 5). The remaining >60 µm fraction was then suspended in 500
159 ml of filtered distilled water (*i.e.* ~1 g L^{-1}) and the resulting solution sonicated at 30 kHz for 5
160 min to dissociate potential aggregates (**Figure 2**, step 6) in order to improve the subsequent
161 second sieving through the 60 µm sieve with filtered 70% ethanol (**Figure 2**, steps 7–8). The
162 60 µm sieve was then dried at 60°C o/n and the dried >60 µm MP fraction was weighed with a
163 digital precision weighing instrument (RADWAG® PS 600.R2; read accuracy = 0.0001 g) by
164 putting the fraction in a tared cup (**Figure 2**, step 8). The MP 20–60 µm fraction was put through
165 the same liquid sieving described above (**Figure 2**, steps 9–12) with the addition of Tween-20®
166 (0.1% of the total volume) to the suspended solution before sonication to improve the final
167 sieving phase. The MP 20–60 µm fraction was then rinsed a last time with filtered 70% ethanol
168 and dried at 60°C o/n before recovery and weighing (**Figure 2**, step 12). The obtained MP 20–
169 60 µm fraction was conserved in stock solution resuspended in filtered ethanol at 1.5 g L^{-1} for
170 particle size distribution and microstructure characterization (**Figure 2**, steps 13–14).
171 All the sieving steps were realised under an extractor hood and over a glass dish. All materials
172 were cleaned and rinsed between each grinding treatment. All wastes, including liquids, were
173 treated as chemical waste.

2.3. Quantitative assessment

Microplastic fractions were weighed to estimate the relative mass of the >60 µm and 20–60 µm fractions as well as the loss of plastic mass following production from an initial 4 g of plastic pieces (*i.e.* 2 g per jar) for each plastic type and grinding condition.

2.4. Particle characterization

Size distributions of the produced MP were assessed using a Multisizer^{TM} 3 Coulter Counter (Beckman Coulter, Inc., Brea, CA) equipped with a 100 µm aperture tube (detection range of 2–100 µm), an approach commonly used to analyse "homemade" microplastics (*e.g.* Schür et al., 2020). A 1.5 µl MP suspension was added to 15 ml electrolytic solution (0.9% NaCl solution) supplied by the manufacturer (Beckman Coulter, Inc., Brea, CA) and previously filtered on a 0.2 µm sterile filter. The solution was shaken before measurement and three repeated measures with the 100 µm capillary (100 µl analytical volume, 300 measured points from 2 to 100 µm size) were performed for each condition. Background measurements were also performed without any MP suspension to quantify contamination in the electrolytic solution. Concentrations and size distribution of microplastics were thus corrected by subtracting the number of particles measured in the electrolytic solution for each of the measured points.

Laser diffraction analyses were also done, using a Beckman Coulter LS 130 particle laser diffractometer (Beckman Coulter, Inc., Brea, CA) to measure the size distribution of the particles down to 0.4 µm. A few ml of stock solutions were injected until an obturation of 5% was reached.

The particle microstructure was observed using a Hitachi TM 3030 scanning electron microscope (SEM) at 15 kV (in charge-up reduction mode) to analyse particle shapes and

structures in dry conditions (on the remaining plastic powder) and following slow solvent (ethanol) evaporation (from resuspended MP stock solution).

2.5. Data analyses

The weights of the microplastic fractions gave the distribution between fractions >60 µm and 20–60 µm, as well as the plastic mass loss caused during the production method, which was calculated by subtracting the weighed MP fractions from the initial weight. Data on particle size distribution obtained by Coulter counter analysis of the 20–60 µm fraction were averaged and plotted on the 300 measured points (from 2 to 100 µm). We determined the proportion of particles really included in the obtained 20–60 µm fraction as well as proportions of particles above and below 60 and 20 µm, respectively. Pairwise comparisons were done to determine significant differences between grinding times regarding frequency distributions of particle count across the size ranges of 2–20 µm and 20–60 µm using Fisher's exact test. Considering no difference, grinding times were then grouped by plastic type and used as replicates (n = 3) to compare the relative abundance of particle count between both size ranges. Data were therefore transformed by the arcsine square root function. Normality of data distribution and homogeneity of variance were tested with Shapiro-Wilk test and Bartlett test, respectively. Means (± standard deviation, SD) were then compared using a two-way ANOVA for plastic type and size range (α = 0.05). Tukey's post hoc test was used to determine the significant differences between the averages of each group. Results were considered significant at $P < 0.05$. Data on the differential volume (%) and number (%) of analysed particles obtained by laser diffraction analysis were plotted on 24 measured points (from 0.375 to 200 µm). The average size (mean ± SD) and relative abundance of total analysed particles in the sizes <1, <10, <20, <50, <100 and <200 µm were obtained. All analyses were performed and graphics drawn in RStudio v4.0.5 statistics software.

3. Results and discussion

3.1. A microplastic production method adaptable to plastic properties

High mass proportions of MP >60 µm were recovered for both types of plastic regardless of the grinding time (**Table 1**). The >60 µm fraction made from the spat collector reached weights of 3.96 g (99.0%), 3.94 g (98.4%) and 3.87 g (96.7%) after 1, 2 and 3 min of grinding, respectively; from the rope the weights were 3.64 g (91.0%), 3.10 g (77.6%) and 3.69 g (92.2%), respectively (**Table 1**). Accordingly, low mass proportions were recovered in the spat collector 20–60 µm fraction, reaching only 0.03 g (0.9%), 0.03 g (0.7%) and 0.03 g (0.8%) after 1, 2 and 3 min of grinding, respectively, while the weight of this fraction from rope reached 0.15 g (3.7%), 0.69 g (17.2%) and 0.16 g (4.0%) for these grinding times (**Table 1**). Interestingly, a greater proportion of MP weight was obtained in PE rope following 2 min grinding before decreasing after 3 min grinding. Even though those results came from single replicate (and were therefore not tested statistically), it is likely that 2 min grinding reached an intermediate state of particle size improving the sieving phase. Indeed, smaller particle size might have favoured their passage through the 60 µm sieve compared to 1 min grinding. Meanwhile, particle size produced might have decreased following 3 min grinding leading to larger and harder formation of aggregates > 60 µm (Hotze et al., 2010; Ashraf et al., 2018). Despite a high variability according to grinding time in the weight of the 20–60 µm fraction in MP made from rope, the mass of these particles was from 5 to 25 times greater than those made from spat collector. In addition, higher mass losses were observed from the rope than from the spat collector (**Table 1**). This plastic mass loss may be explained in several ways, including the sticking of particles to lab materials, particle volatility or the production of small MP <20 µm. In view of these results, grinding time seems to have a low influence on the production of 20–60 µm particles and on the loss of plastic mass, and these effects are clearly smaller than the influence of plastic

type. Differences in grinding fractions between spat collector and rope could be related to plastic type properties including density, crystallinity and additive content as well as shape and weathering. Indeed, even though liquid nitrogen makes plastic matter more brittle, grinding efficiency may be influenced by plastic density (*i.e.* by taking more or less space in the grinding jar and thus affecting mechanical grinding), which was higher for rope than spat collector (jar $\text{filling}_{\text{coll}}$ > jar $\text{filling}_{\text{rope}}$). It may also be influenced by the shape of the plastic pieces before grinding, which was quite flat and thin for spat collector but cylindrical and thicker for rope (**Figure 1**C and F), favouring fragmentation in the latter (Oyinloye and Yoon, 2020). In addition, the grinding efficiency of plastic types is likely influenced by their intrinsic mechanical resistance, which is partly dependent on the additives incorporated during their manufacture (*e.g.* plasticisers, antioxidants), and their weathering at sea, characterized by the loss of structural integrity induced by biotic (*i.e.* biodegradation) and abiotic (*e.g.* photolysis, hydrolysis, thermal degradation) factors (Andrady, 2011), including the leaching of additives (Hahladakis et al., 2018). For example, phthalate esters, such as bis(2-ethylhexyl) phthalate (DEHP), are commonly used as plasticisers to improve the quality and durability of polymers by increasing their flexibility (Rowdhwal and Chen, 2018). A previous study showed DEHP to be one of the most important plastic additives in both plastic types, with a higher concentration quantified in aged rope (95.51 µg g^{-1}) than spat collector (70.26 µg g^{-1}) (Gardon et al., 2020a). It is likely that differences in concentrations of DEHP and/or other specific additives might have influenced the mechanical resistance of both plastic types to cryogrinding. Therefore, it seems that the mechanical properties of plastic materials, their fate and, probably, their ageing are important factors to consider in the choice of grinding time, both to limit the loss of materials and optimize the yield of the targeted size range fraction. In our study, ageing was probably not a driving variable as the infrared spectra did not show strong oxidation of the collected polymers. Indeed, the carbonyl absorption band in the 1780–1660 cm^{-1} region, which can be

used as a probe to monitor surface oxidation of PE and PP (Rowenczyk et al., 2020), remained weak (**Figure 1**A–B).

3.2. Inconsistency between particle sieving range and actual size distribution

Size distribution analyses of the 20–60 µm fractions revealed an inconsistency between the theoretical sieving range and the actual particle sizes, regardless of the plastic type or grinding time. The effectiveness of the protocol was shown by the increased number of MP in the range from 20 µm (~130–870 MP μg^{-1}) to 60 µm (~0–130 MP μg^{-1}) according to the Coulter counter analyses (**Figure 3**A–B, focusing on the particle size distribution in the range of 4–60 µm). The peak particle number appeared to be mostly centred around 20 µm. However, there was a decrease in particle frequency around 8 µm, and further down, a large increase in the number of particles of smaller size (around 5 µm and below; **Figure 3**A–B). Coulter counter analyses (only considering particles >2 µm) showed that the actual 20–60 µm fractions only reached 5.7% (~26,000 MP μg^{-1}), 17.8% (~28,000 MP μg^{-1}) and 16.1% (~28,000 MP μg^{-1}) of the total analysed particles from PP spat collector after 1, 2 and 3 min of grinding, respectively; and 3.6% (~17,000 MP μg^{-1}), 6.1% (~18,000 MP μg^{-1}) and 8.4% (~18,000 MP μg^{-1}) from PE rope, respectively (**Table 2**). No difference occurred between grinding times in the frequency distributions of particles across size ranges of 2–20 µm and 20–60 µm ($P > 0.05$). Using grinding times as replicates ($n = 3$), the relative abundance of particle count in the 20–60 µm fraction reached 13.2 ± 6.6% and 6.0 ± 2.4% for PP spat collector and PE rope, respectively; while averages in the 2–20 µm fraction reached 86.8 ± 6.6% and 94.0 ± 2.4%, respectively. No significant difference was observed between plastic types according to size range. However, a significant lower number of particles ($P < 0.0001$) was obtained in the 20–60 µm fraction compared to the 2–20 µm fraction (**Figure 3**C). Particle size characterization therefore demonstrated that 53–70% (~82,000–333,000 MP μg^{-1}) of the total analysed particles in the 20–60 µm fractions were in fact <3 µm (**Table 2**). Such a result indicates the potential

occurrence of the smallest MP and nanoplastics (MNP) in the 20 µm sieved plastic powder despite all precautions taken to dispose of MP <20 µm (*i.e.* liquid sieving, sonication steps and the use of Tween-20® dispersing agent). Considering the similar Coulter counter results among the different grinding times, we focused our laser diffraction analyses on the 1-min grinding treatment, which confirmed and fine-tuned particle size distribution (considering particles >0.4 µm; **Figure 4**). Results showed a high number of particles below the 2 µm threshold, with 89.1% (0.70 ± 0.75 µm) and 81.6% (0.82 ± 1.02 µm) of total particles <1 µm from spat collector and rope, respectively (**Figure 4**A and C). It demonstrates the gap between a conventionally used method (*i.e.* a Coulter counter) to characterize particle size distribution up to the 2 µm threshold (*e.g.* Schür et al., 2020) and a finer analysis including the nano fraction capable of detecting particles up to the 0.4 µm threshold (Balakrishnan et al., 2020). This gap emphasizes the need to be very cautious when assessing particle size distribution on a volume or number basis. Considering that small particles will count very little in terms of volume/weight, but a great deal in terms of numbers (**Figure 4**), it clearly appears that their presence should not be ignored, especially when conducting ecotoxicological studies. Overall, our results highlighted the discrepancy between what is expected from the sieving and what is really obtained in the relevant fractions. Such data confirm the need to thoroughly check the size distribution of "homemade" MP using appropriate analytical methods for both micro- and nanosized particles.

3.3. Particle self-assembly induces biased sieving and size assessment

A plausible explanation for the observed sieving inefficiency is the formation of anisotropic assemblies, in which physical properties of particles differ according to their orientation. Such phenomenon has already been demonstrated by spherical NP uniformly grafted with macroparticles that robustly self-assemble into a variety of anisotropic superstructures when they are dispersed in the corresponding polymer matrix (Akcora et al., 2009; Damasceno et al., 2012). Self-assembly is the process by which individual components arrange themselves into

an ordered structure. Self-assemblies and particle interactions are probably less frequent when a polymer matrix is diluted during size characterization (Jain et al., 2004), making it possible to observe these diverging results between quantitative and qualitative assessments. This physical phenomenon is likely illustrated by our results on size distribution obtained with the Coulter counter, which showed totals of 6,800, 2,300 and 2,600 analysed particles from spat collector samples after 1-, 2- and 3-min runs, respectively (**Figure 3**A), and 7,200, 4,500 and 3,300 from the rope samples (**Figure 3**B). Even though those results came from pseudo-replicates, the number of analysed particles was higher after 1 min of grinding than after 2 and 3 min with either plastic type, suggesting a large amount of particle self-assembly, possibly depending on the size reduction induced by the longer grinding time. The formation of aggregates in the MP 20–60 µm fraction was confirmed by laser diffraction analyses showing 4% and 14% of total volume particles >60 µm from spat collector (**Figure 4**B) and rope (**Figure 4**D) samples, respectively. Characteristics such as shape, surface properties, charge, polarizability or mass could determine the degree of self-assembly, producing structures and patterns at all physical scales (Whitesides and Grzybowski, 2002). Molecular mechanisms involved in self-assembly include non-covalent or weak-covalent interactions such as van der Waals, electrostatic and hydrophobic interactions (Whitesides and Grzybowski, 2002; Deng et al., 2020). According to our results, these interactions may be plastic type-dependent (Yanar and Kwetkus, 1995; Park et al., 2008) as well as influenced by particle shape and size (Damasceno et al., 2012). Spontaneous MP self-assembly into crystal superstructures could explain why the sieving was not sufficiently effective (Lee et al., 2018; Deng et al., 2020), as illustrated in the SEM images (**Figure 5**). This physical phenomenon may have occurred between the drying phase (**Figure 5**A–B) and the liquid sieving phase over the 20 µm sieve of which the ethanol efflux was slow. This condition could be compared to the solvent evaporation-driven assembly system developed by Lee et al. (2018) (**Figure 5**C–I). It seems

345 that the sonicating bath containing Tween-20® did not have the expected effect of preventing
346 particle aggregation, as illustrated by the formation of 3D crystals of cuboid shape on all
347 physical scales (**Figure 5**C–H). Further research and development are needed to reduce these
348 particle interactions in polymer matrices to dispose of more of the MP <20 µm and get as close
349 as possible to the desired size range. A promising investigation way is the introduction of
350 stabiliser/protectant that plays an active part in preventing hard agglomerate formation during
351 the drying process (Yeap, 2018). For example, De Jaeghere et al. (1999) examined the re-
352 dispersibility of suspended polyethylene oxide-grafted nanoparticles previously frozen into ice
353 crystals before subjecting to lyophilization with and without lyoprotectant (trehalose). Results
354 showed that lyophilized nanoparticles without trehalose was found to form agglomerates even
355 after sonication for re-dispersion procedure. Meanwhile, the ability of lyophilized nanoparticles
356 with trehalose to be re-dispersed was significantly enhanced. In this study, we have therefore
357 demonstrated the necessity of considering size distribution as well as the total number of
358 particles and aggregates, since the aggregates are not dissociated during the measurement
359 process.

360 Here, we emphasised the importance to better understand MNP fate and behaviour aiming to
361 control particle size distribution in the corresponding polymer matrix. This constitutes a
362 preliminary step towards the description of more complex aquatic system, such as experimental
363 conditions involving more than two components interacting with one another, such as
364 microalgae (Demir-Yilmaz et al., 2022), and/or by considering natural organic matter as small
365 aggregates already present in the dispersing medium (Clavier et al., 2019). This can result in a
366 complex combination of homo- and heteroaggregates (Praetorius et al., 2020), especially in
367 marine water where all particle contacts are effective due to high ionic strength promoting
368 various aggregation pathways and several possible attachment efficiencies (Clavier et al.,
369 2019). These complex interactions make their theoretical and experimental determination

challenging (Praetorius et al., 2020), while their influence on exposure parameters remain concrete on bioavailability in ecotoxicological studies.

3.4. Implications for ecotoxicological studies

In this study, we attempted to produce MP in a range of 20 to 60 µm in order to match the retention size range of *P. margaritifera* (*i.e.* 2–200 µm) (Pouvreau et al., 1999), which would enable controlled exposition in future experiments. Particle characterization revealed that the MP produced by our method were ≤60 µm, but results demonstrated an uncontrolled production of MP <20 µm, mainly because of particles smaller than 1 µm (>80% of the total particle number). This experimental artefact raises important questions for the interpretation of previously published result from (eco)toxicological studies that used grinding and sieving methods to produce MP without thoroughly characterizing the size range of the particles in the nanometric range (*e.g.* Schür et al., 2020). Some authors mention such bias to interpreting their toxicological data, as illustrated by Revel et al. (2019), who discussed a possible implication of NP in the observed toxicity with regards to their MP production method. Whenever possible, the proportion of small MP and NP must be characterized and considered in the exposition levels, especially with regard to the hypothesis that particle toxicity increases as size decreases (Jeong et al., 2016; Ma et al., 2016). This is a real problem for assessing the toxicity of MNP to obtain relevant data for decision support, but also because no data is available regarding *in situ* NP contamination (Schwaferts et al., 2019). In addition, the lack of consideration of the smallest particle sizes also raises an ethical issue associated to pollution with the possible release of NP in wastewater effluents from experiments. Indeed, NP may pass through most of the filtration devices, therefore entering the natural environment (Paul-Pont et al., 2018).

Overall, our study highlights that controlling the size distributions of small MP and NP following laboratory MP production poses some significant challenges since their hierarchical

394 self-assembly remains a physical problem. While waiting for better knowledge of *in situ*
395 contamination, there is an important need to improve particle production methodology and
396 associated characterization of particle populations.

397 Author information

398 Corresponding Author

399 *Phone: (+689) 40 54 60 47. Fax: (+689) 40 54 60 99. E-mail: tony.gardon@ifremer.fr

400 ORCID

401 Tony Gardon: 0000-0002-5761-0526

402 Notes

403 The authors declare no competing financial interest

404 Acknowledgments

405 This study was financially supported by the MICROLAG project funded by *Direction des*
406 *Ressources Marines* (DRM) of French Polynesia and by the European INTERREG France
407 (Channel) England project "Preventing Plastic Pollution" co-financed by the European
408 Regional Development Fund. T. Gardon was funded by a doctoral research grant N°09793 from
409 Ifremer. We would like to thank the *Institut de Radioprotection et de Sûreté Nucléaire* (IRSN)
410 of French Polynesia for supplying liquid nitrogen, particularly Patrick Bouisset (Laboratory of
411 Environment Study and Monitoring – IRSN – LESE).

References

Akcora, P., Liu, H., Kumar, S.K., Moll, J., Li, Y., Benicewicz, B.C., Schadler, L.S., Acehan, D., Panagiotopoulos, A.Z., Pryamitsyn, V., Ganesan, V., Ilavsky, J., Thiyagarajan, P., Colby, R.H., Douglas, J.F., 2009. Anisotropic self-assembly of spherical polymer-grafted nanoparticles. Nature Mater 8, 354–359. https://doi.org/10.1038/nmat2404

Andrady, A.L., 2011. Microplastics in the marine environment. Marine Pollution Bulletin 62, 1596–1605. https://doi.org/10.1016/j.marpolbul.2011.05.030

Andréfouët, S., Thomas, Y., Lo, C., 2014. Amount and type of derelict gear from the declining black pearl oyster aquaculture in Ahe atoll lagoon, French Polynesia. Marine Pollution Bulletin 83, 224–230. https://doi.org/10.1016/j.marpolbul.2014.03.048

Ashraf, M.A., Peng, W., Zare, Y., Rhee, K.Y., 2018. Effects of Size and Aggregation/Agglomeration of Nanoparticles on the Interfacial/Interphase Properties and Tensile Strength of Polymer Nanocomposites. Nanoscale Research Letters 13, 214. https://doi.org/10.1186/s11671-018-2624-0

Balakrishnan, G., Lagarde, F., Chassenieux, C., Nicolai, T., 2020. Characterisation of Colloidal Particles in Seawater by Light Scattering Techniques. https://doi.org/10.20944/preprints202003.0189.v1

Carrasco-Navarro, V., Muñiz-González, A.-B., Sorvari, J., Martínez-Guitarte, J.-L., 2021. Altered gene expression in *Chironomus riparius* (insecta) in response to tire rubber and polystyrene microplastics. Environmental Pollution 285, 117462. https://doi.org/10.1016/j.envpol.2021.117462

Clavier, A., Praetorius, A., Stoll, S., 2019. Determination of nanoparticle heteroaggregation attachment efficiencies and rates in presence of natural organic matter monomers. Monte Carlo modelling. Science of The Total Environment 650, 530–540. https://doi.org/10.1016/j.scitotenv.2018.09.017

Cole, M., 2016. A novel method for preparing microplastic fibers. Sci Rep 6, 34519. https://doi.org/10.1038/srep34519

Connors, K.A., Dyer, S.D., Belanger, S.E., 2017. Advancing the quality of environmental microplastic research: Advancing the quality of environmental microplastic research. Environ Toxicol Chem 36, 1697–1703. https://doi.org/10.1002/etc.3829

Cózar, A., Echevarria, F., Gonzalez-Gordillo, J.I., Irigoien, X., Ubeda, B., Hernandez-Leon, S., Palma, A.T., Navarro, S., Garcia-de-Lomas, J., Ruiz, A., Fernandez-de-Puelles, M.L., Duarte, C.M., 2014. Plastic debris in the open ocean. Proceedings of the National Academy of Sciences 111, 10239–10244. https://doi.org/10.1073/pnas.1314705111

Damasceno, P.F., Engel, M., Glotzer, S.C., 2012. Predictive Self-Assembly of Polyhedra into Complex Structures. Science 337, 453–457. https://doi.org/10.1126/science.1220869

De Jaeghere, F., Allémann, E., Leroux, J.C., Stevels, W., Feijen, J., Doelker, E., Gurny, R., 1999. Formulation and lyoprotection of poly(lactic acid-co-ethylene oxide) nanoparticles: influence on physical stability and in vitro cell uptake. Pharm Res 16, 859–866. https://doi.org/10.1023/a:1018826103261

de Sá, L.C., Oliveira, M., Ribeiro, F., Rocha, T.L., Futter, M.N., 2018. Studies of the effects of microplastics on aquatic organisms: What do we know and where should we focus our efforts in the future? Science of The Total Environment 645, 1029–1039. https://doi.org/10.1016/j.scitotenv.2018.07.207

Demir-Yilmaz, I., Yakovenko, N., Roux, C., Guiraud, P., Collin, F., Coudret, C., ter Halle, A., Formosa-Dague, C., 2022. The role of microplastics in microalgae cells aggregation: A study at the molecular scale using atomic force microscopy. Science of The Total Environment 832, 155036. https://doi.org/10.1016/j.scitotenv.2022.155036

Deng, K., Luo, Z., Tan, L., Quan, Z., 2020. Self-assembly of anisotropic nanoparticles into functional superstructures. Chem. Soc. Rev. 49, 6002–6038. https://doi.org/10.1039/D0CS00541J

Eitzen, L., Paul, S., Braun, U., Altmann, K., Jekel, M., Ruhl, A.S., 2019. The challenge in preparing particle suspensions for aquatic microplastic research. Environ Res 168, 490–495. https://doi.org/10.1016/j.envres.2018.09.008

El Hadri, H., Gigault, J., Maxit, B., Grassl, B., Reynaud, S., 2020. Nanoplastic from mechanically degraded primary and secondary microplastics for environmental assessments. NanoImpact 17, 100206. https://doi.org/10.1016/j.impact.2019.100206

Eriksen, M., Lebreton, L.C.M., Carson, H.S., Thiel, M., Moore, C.J., Borerro, J.C., Galgani, F., Ryan, P.G., Reisser, J., 2014. Plastic Pollution in the World's Oceans: More than 5 Trillion Plastic Pieces Weighing over 250,000 Tons Afloat at Sea. PLoS ONE 9, e111913. https://doi.org/10.1371/journal.pone.0111913

Gardon, T., El Rakwe, M., Paul-Pont, I., Le Luyer, J., Thomas, L., Prado, E., Boukerma, K., Cassone, A.-L., Quillien, V., Soyez, C., Costes, L., Crusot, M., Dreanno, C., Le Moullac, G., Huvet, A., 2021. Microplastics contamination in pearl-farming lagoons of French Polynesia. Journal of Hazardous Materials 126396. https://doi.org/10.1016/j.jhazmat.2021.126396

Gardon, T., Huvet, A., Paul-Pont, I., Cassone, A.-L., Sham Koua, M., Soyez, C., Jezequel, R., Receveur, J., Le Moullac, G., 2020a. Toxic effects of leachates from plastic pearl-farming gear on embryo-larval development in the pearl oyster *Pinctada margaritifera*. Water Research 179, 115890. https://doi.org/10.1016/j.watres.2020.115890

Gardon, T., Morvan, L., Huvet, A., Quillien, V., Soyez, C., Le Moullac, G., Le Luyer, J., 2020b. Microplastics induce dose-specific transcriptomic disruptions in energy metabolism and immunity of the pearl oyster *Pinctada margaritifera*. Environmental Pollution 266, 115180. https://doi.org/10.1016/j.envpol.2020.115180

Gardon, T., Reisser, C., Soyez, C., Quillien, V., Le Moullac, G., 2018. Microplastics Affect Energy Balance and Gametogenesis in the Pearl Oyster *Pinctada margaritifera*. Environmental Science & Technology. https://doi.org/10.1021/acs.est.8b00168

Hahladakis, J.N., Velis, C.A., Weber, R., Iacovidou, E., Purnell, P., 2018. An overview of chemical additives present in plastics: Migration, release, fate and environmental impact during their use, disposal and recycling. Journal of Hazardous Materials 344, 179–199. https://doi.org/10.1016/j.jhazmat.2017.10.014

Hotze, E.M., Phenrat, T., Lowry, G.V., 2010. Nanoparticle Aggregation: Challenges to Understanding Transport and Reactivity in the Environment. Journal of Environmental Quality 39, 1909–1924. https://doi.org/10.2134/jeq2009.0462

Jahnke, A., Arp, H.P.H., Escher, B.I., Gewert, B., Gorokhova, E., Kühnel, D., Ogonowski, M., Potthoff, A., Rummel, C., Schmitt-Jansen, M., Toorman, E., MacLeod, M., 2017. Reducing Uncertainty and Confronting Ignorance about the Possible Impacts of Weathering Plastic in the Marine Environment. Environmental Science & Technology Letters 4, 85–90. https://doi.org/10.1021/acs.estlett.7b00008

Jain, N., Trabelsi, S., Guillot, S., McLoughlin, D., Langevin, D., Letellier, P., Turmine, M., 2004. Critical Aggregation Concentration in Mixed Solutions of Anionic Polyelectrolytes and Cationic Surfactants. Langmuir 20, 8496–8503. https://doi.org/10.1021/la0489918

Jeong, C.-B., Won, E.-J., Kang, H.-M., Lee, M.-C., Hwang, D.-S., Hwang, U.-K., Zhou, B., Souissi, S., Lee, S.-J., Lee, J.-S., 2016. Microplastic Size-Dependent Toxicity, Oxidative Stress Induction, and p-JNK and p-p38 Activation in the Monogonont Rotifer (*Brachionus koreanus*). Environmental Science & Technology 50, 8849–8857. https://doi.org/10.1021/acs.est.6b01441

Kühn, S., van Oyen, A., Booth, A.M., Meijboom, A., van Franeker, J.A., 2018. Marine microplastic: Preparation of relevant test materials for laboratory assessment of ecosystem impacts. Chemosphere 213, 103–113. https://doi.org/10.1016/j.chemosphere.2018.09.032

Lee, Y.H., Lay, C.L., Shi, W., Lee, H.K., Yang, Y., Li, S., Ling, X.Y., 2018. Creating two self-assembly micro-environments to achieve supercrystals with dual structures using polyhedral nanoparticles. Nat Commun 9, 2769. https://doi.org/10.1038/s41467-018-05102-x

Lenz, R., Enders, K., Nielsen, T.G., 2016. Microplastic exposure studies should be environmentally realistic. Proc Natl Acad Sci USA 113, E4121–E4122. https://doi.org/10.1073/pnas.1606615113

Ma, Y., Huang, A., Cao, S., Sun, F., Wang, L., Guo, H., Ji, R., 2016. Effects of nanoplastics and microplastics on toxicity, bioaccumulation, and environmental fate of phenanthrene in fresh water. Environmental Pollution 219, 166–173. https://doi.org/10.1016/j.envpol.2016.10.061

Oyinloye, T.M., Yoon, W.B., 2020. Effect of Freeze-Drying on Quality and Grinding Process of Food Produce: A Review. Processes 8, 354. https://doi.org/10.3390/pr8030354

Park, C.-H., Jeon, H.-S., Yu, H.-S., Han, O.-H., Park, J.-K., 2008. Application of Electrostatic Separation to the Recycling of Plastic Wastes: Separation of PVC, PET, and ABS. Environ. Sci. Technol. 42, 249–255. https://doi.org/10.1021/es070698h

Paul-Pont, I., Tallec, K., Gonzalez-Fernandez, C., Lambert, C., Vincent, D., Mazurais, D., Zambonino-Infante, J.-L., Brotons, G., Lagarde, F., Fabioux, C., Soudant, P., Huvet, A., 2018. Constraints and Priorities for Conducting Experimental Exposures of Marine Organisms to Microplastics. Front. Mar. Sci. 5. https://doi.org/10.3389/fmars.2018.00252

Phuong, N.N., Zalouk-Vergnoux, A., Poirier, L., Kamari, A., Châtel, A., Mouneyrac, C., Lagarde, F., 2016. Is there any consistency between the microplastics found in the field and those used in laboratory experiments? Environmental Pollution 211, 111–123. https://doi.org/10.1016/j.envpol.2015.12.035

Pouvreau, S., Jonquières, G., Buestel, D., 1999. Filtration by the pearl oyster, Pinctada margaritifera, under conditions of low seston load and small particle size in a tropical lagoon habitat. Aquaculture 176, 295–314. https://doi.org/10.1016/S0044-8486(99)00102-7

Praetorius, A., Badetti, E., Brunelli, A., Clavier, A., Alberto Gallego-Urrea, J., Gondikas, A., Hassellöv, M., Hofmann, T., Mackevica, A., Marcomini, A., Peijnenburg, W., K. Quik, J.T., Seijo, M., Stoll, S., Tepe, N., Walch, H., Kammer, F. von der, 2020. Strategies for determining heteroaggregation attachment efficiencies of engineered nanoparticles in aquatic environments. Environmental Science: Nano 7, 351–367. https://doi.org/10.1039/C9EN01016E

Revel, M., Lagarde, F., Perrein-Ettajani, H., Bruneau, M., Akcha, F., Sussarellu, R., Rouxel, J., Costil, K., Decottignies, P., Cognie, B., Châtel, A., Mouneyrac, C., 2019. Tissue-Specific Biomarker Responses in the Blue Mussel *Mytilus spp.* Exposed to a Mixture of Microplastics at Environmentally Relevant Concentrations. Front. Environ. Sci. 7. https://doi.org/10.3389/fenvs.2019.00033

Rochman, C.M., Brookson, C., Bikker, J., Djuric, N., Earn, A., Bucci, K., Athey, S., Huntington, A., McIlwraith, H., Munno, K., Frond, H.D., Kolomijeca, A., Erdle, L., Grbic, J., Bayoumi, M., Borrelle, S.B., Wu, T., Santoro, S., Werbowski, L.M., Zhu, X., Giles, R.K., Hamilton, B.M., Thaysen, C., Kaura, A., Klasios, N., Ead, L., Kim, J., Sherlock, C., Ho, A., Hung, C., 2019. Rethinking microplastics as a diverse contaminant

559 suite. Environmental Toxicology and Chemistry 38, 703–711.
560 https://doi.org/10.1002/etc.4371
561 Rowdhwal, S.S.S., Chen, J., 2018. Toxic Effects of Di-2-ethylhexyl Phthalate: An Overview.
562 BioMed Research International 2018, e1750368. https://doi.org/10.1155/2018/1750368
563 Schür, C., Zipp, S., Thalau, T., Wagner, M., 2020. Microplastics but not natural particles induce
564 multigenerational effects in *Daphnia magna*. Environmental Pollution 260, 113904.
565 https://doi.org/10.1016/j.envpol.2019.113904
566 Schwaferts, C., Niessner, R., Elsner, M., Ivleva, N.P., 2019. Methods for the analysis of
567 submicrometer- and nanoplastic particles in the environment. TrAC Trends in
568 Analytical Chemistry 112, 52–65. https://doi.org/10.1016/j.trac.2018.12.014
569 Thornton Hampton, L.M., Lowman, H., Coffin, S., Darin, E., De Frond, H., Hermabessiere, L.,
570 Miller, E., de Ruijter, V.N., Faltynkova, A., Kotar, S., Monclús, L., Siddiqui, S., Völker,
571 J., Brander, S., Koelmans, A.A., Rochman, C.M., Wagner, M., Mehinto, A.C., 2022. A
572 living tool for the continued exploration of microplastic toxicity. Microplastics and
573 Nanoplastics 2, 13. https://doi.org/10.1186/s43591-022-00032-4
574 van Sebille, E., Wilcox, C., Lebreton, L., Maximenko, N., Hardesty, B.D., van Franeker, J.A.,
575 Eriksen, M., Siegel, D., Galgani, F., Law, K.L., 2015. A global inventory of small
576 floating plastic debris. Environmental Research Letters 10, 124006.
577 https://doi.org/10.1088/1748-9326/10/12/124006
578 Whitesides, G.M., Grzybowski, B., 2002. Self-assembly at all scales. Science 295, 2418–2421.
579 https://doi.org/10.1126/science.1070821
580 Woodall, L.C., Sanchez-Vidal, A., Canals, M., Paterson, G.L.J., Coppock, R., Sleight, V.,
581 Calafat, A., Rogers, A.D., Narayanaswamy, B.E., Thompson, R.C., 2014. The deep sea
582 is a major sink for microplastic debris. Royal Society Open Science 1, 140317–140317.
583 https://doi.org/10.1098/rsos.140317
584 Yanar, D.K., Kwetkus, B.A., 1995. Electrostatic separation of polymer powders. Journal of
585 Electrostatics, Selected papers from the special technical session “Electrostatics in
586 Polymer Processing and Charge Monitoring”, 1993 IEEE Industry Applications Society
587 Meeting 35, 257–266. https://doi.org/10.1016/0304-3886(94)00044-W
588 Yeap, S.P., 2018. Permanent agglomerates in powdered nanoparticles: Formation and future
589 prospects. Powder Technology 323, 51–59.
590 https://doi.org/10.1016/j.powtec.2017.09.042
591 Zimmermann, L., Göttlich, S., Oehlmann, J., Wagner, M., Völker, C., 2020. What are the
592 drivers of microplastic toxicity? Comparing the toxicity of plastic chemicals and
593 particles to *Daphnia magna*. Environmental Pollution 267, 115392.
594 https://doi.org/10.1016/j.envpol.2020.115392
595

596

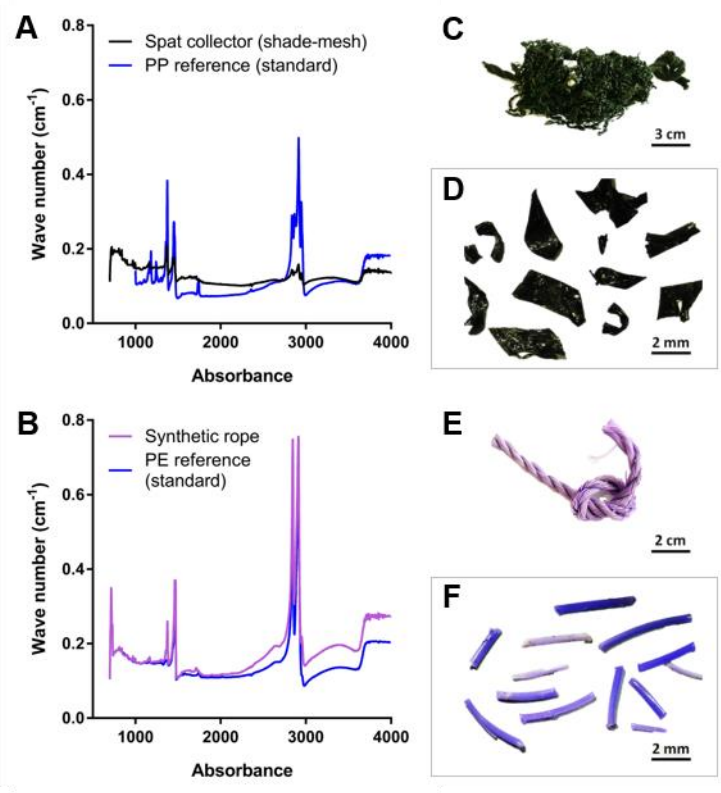

Figure 1. Polymer identification in two plastic pearl farming gear types by FTIR. Polypropylene (PP) for the spat collector (A) and polyethylene (PE) for the synthetic rope (B). Photographs show the spat collector (C) and synthetic rope (E) and their associated plastic pieces (D and F, respectively) used for MP production. Spectra of particles produced were identical to those of plastic gears, hence not added here. Adapted from Gardon et al. (2020a).

605

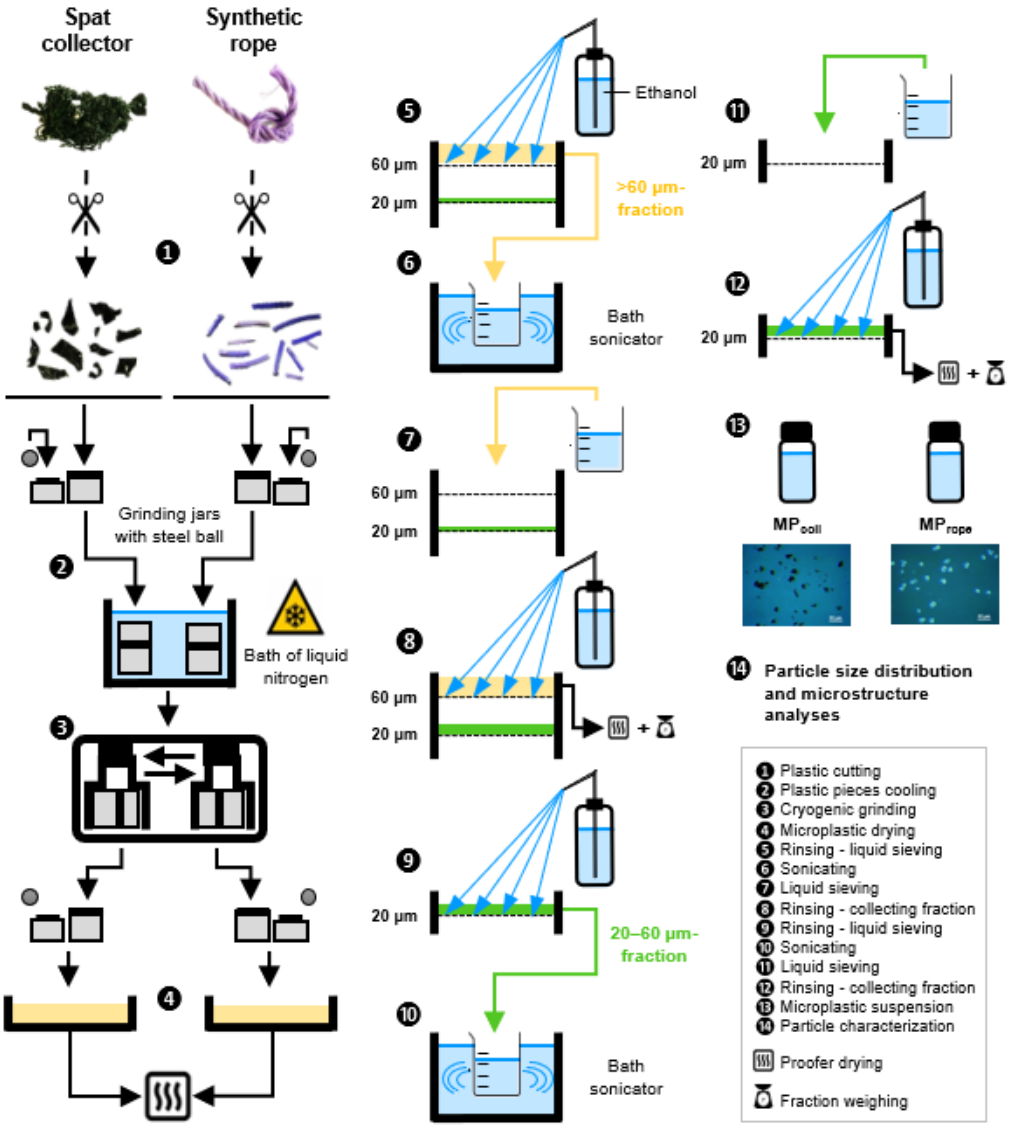

606

607 **Figure 2.** Synthetic diagram of the microplastic production method tested.

608

609 **Table 1.** Microplastic fractions produced from the two types of plastic pearl farming gear
610 according to grinding time.

Grinding time	MP fraction	Plastic type			
		PP spat collector		**PE rope**	
		Weight (g)	Proportion (%)	Weight (g)	Proportion (%)
Initial		4.0000	100.0	4.0000	100.0
1 min	**>60 µm**	3.9588	99.0	3.6410	91.0
	20–60 µm	0.0344	0.9	0.1490	3.7
	Loss*	0.0068	0.2	0.2100	5.2
2 min	**>60 µm**	3.9377	98.4	3.1050	77.6
	20–60 µm	0.0295	0.7	0.6900	17.2
	Loss*	0.0328	0.8	0.2050	5.1
3 min	**>60 µm**	3.8676	96.7	3.6890	92.2
	20–60 µm	0.0305	0.8	0.1620	4.0
	Loss*	0.1019	2.5	0.1490	3.7

611

612 * The loss of plastic mass was calculated by subtracting the weighed MP fractions from the
613 initial 4.00 g of plastic pieces.

614

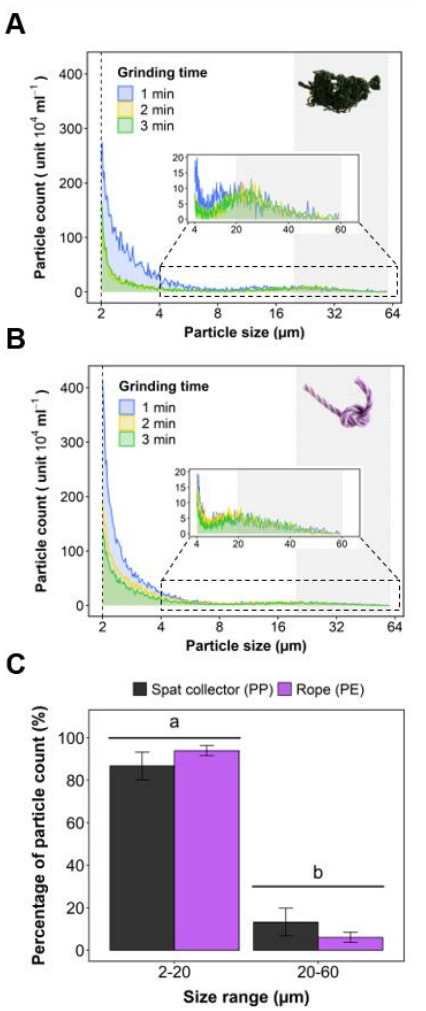

Figure 3. Particle size distribution of microplastics obtained in the 20–60 µm fraction as assessed by Coulter counter analyses. Density plots of particle size distribution of MP 20–60 µm fraction obtained from spat collector (A) and rope (B) samples according to grinding times of 1, 2 and 3 minutes. Bar chart of the relative abundance of particle count across size ranges of 2–20 µm and 20–60 µm according to plastic type (C). The dashed black line on the density plots indicates the minimal 2 µm detection thresholds from the Coulter counter (equipped with a 100 µm aperture tube) analysis. The grey area corresponds to the 20 to 60 µm sieving range used in the present microplastic production method. Bar chart illustrate mean ± SD with grinding times as replicates (n = 3). Letters indicate statistically significant differences between groups.

627 **Table 2.** Relative abundance of microplastics produced in the 20–60 µm fraction according to

628 their size distribution above the 2 µm threshold.

Plastic type	Grinding time	Percentage of particle count (%)				
		2-3 µm	**<5 µm**	**<10 µm**	**<20 µm**	**20–60 µm**
PP spat collector	**1 min**	62	82	88	94	6
	2 min	53	66	71	82	18
	3 min	56	69	74	84	16
PE rope	**1 min**	70	88	92	96	4
	2 min	60	80	87	94	6
	3 min	60	79	84	92	8

629

630

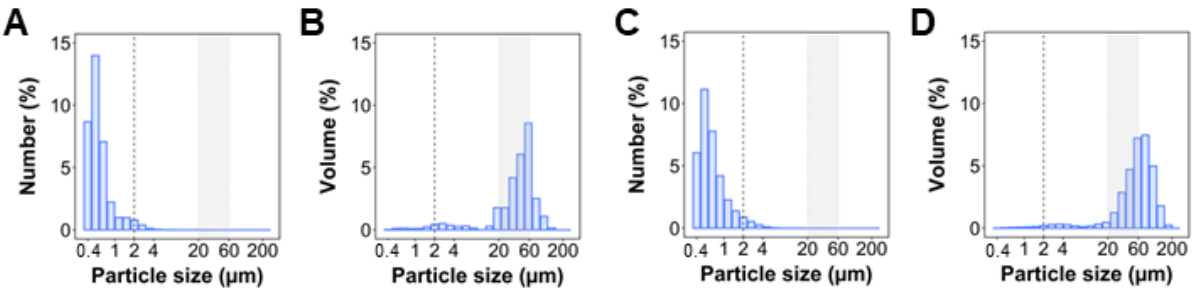

Figure 4. Particle size distribution of microplastics obtained in the 20–60 µm fraction as assessed by laser diffraction analyses. Bar plots (A–D) show the differences in number and volume of particle sizes made from spat collector (A–B) and rope (C–D) by 1 min of grinding. The dashed black line indicates the minimal 2 µm detection thresholds from the Coulter counter (equipped with a 100 µm aperture tube). The grey area corresponds to the 20 to 60 µm sieving range used in the present microplastic production method.

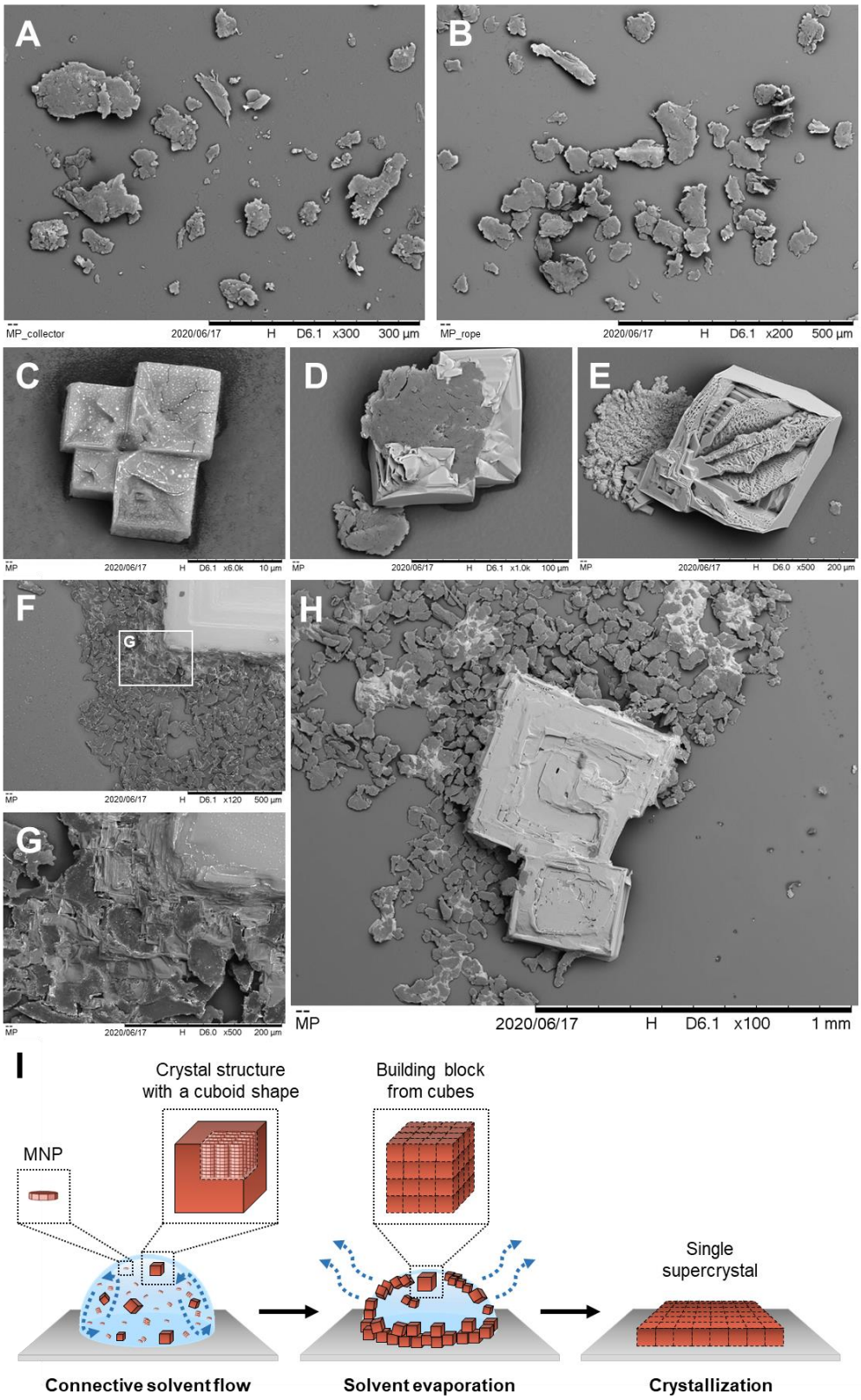

Figure 5. Representative SEM images of microplastics in the 20–60 µm fraction produced in this study and their spontaneous self-assembly into crystal superstructures through slow solvent

644 evaporation. Pictures of MP made from spat collector (A) and rope (B) samples taken in dry
645 conditions. Pictures of ordered assemblies from colloidal micro- and nanoplastics (MNP) of
646 various shapes into crystalline structures with a cuboid shape at all physical scales (C–H). These
647 spontaneous assemblies are associated with attractive forces among particles (*e.g.* van der
648 Waals forces, electrostatic, hydrophobic interactions) and ligand–substrate interactions (*e.g.*
649 chemisorption) responsible for forcing particles to self-arrange into ordered assemblies with
650 multi-layered superstructures (F–G). Connective flow during solvent evaporation concentrates
651 plastic particles and 3D crystals near the drying front, giving rise to building blocks that grow
652 to larger dimensions until complete solvent evaporation occurs and supercrystals form at the
653 millimetric scale (H). A synthetic scheme adapted and redrawn from Lee et al. (2018) and Deng
654 et al. (2020) illustrates this process (I).

655